Collisionally Assisted Spectroscopy of Water from 27 000 to 34 000 cm^{-1}

Maxim Grechko,[†] Pavlo Maksyutenko,[†] Nikolai F. Zobov,[‡] Sergei V. Shirin,[‡] Oleg L. Polyansky,[‡] Thomas R. Rizzo,[†] and Oleg V. Boyarkin[†,*]

Laboratoire de Chimie Physique Moléculaire, École Polytechnique Fédérale de Lausanne, Station 6, CH-1015 Lausanne, Switzerland, and Institute of Applied Physics RAS, Uljanov str. 46, 603950 N-Novgorod, Russia

Received: July 03, 2008; Revised Manuscript Received: August 14, 2008

We report here an experimental approach that enables measurement of weak transitions to a wide range of rovibrational levels of water in the energy region 27 000−34 200 cm^{-1}. We have previously demonstrated the use of laser double-resonance overtone excitation to access highly excited vibrational levels from single rovibrational states. Although this approach simplifies the assignment of the spectra, it strongly reduces the number of observed transitions and hence our ability to test theoretical predictions. Here, we increase significantly the number of observed transitions by allowing rotational relaxation of H_2O at intermediate levels of the double-resonance excitation scheme to the levels of the same nuclear spin (ortho or para). Our recently developed semiempirical potential energy surface PES_{12} enables assignment of the resulting complex spectra and reproduction of the measured transitions with accuracy better than 1 cm^{-1}.

Introduction

Water is clearly a molecule of fundamental importance—being the most abundant on Earth and essential to the functioning of biological systems. Atmospheric water vapor is the major absorber of solar radiation and the most important greenhouse gas.[1] The direct relevance of water to global warming alone has motivated extensive experimental and theoretical studies of its rovibrational spectroscopy. Moreover, its small size and relatively small number of electrons facilitate accurate theoretical treatment, making it a convenient benchmark for testing computational approaches.[2,3]

In the 1930s, Mecke and co-workers[4,5] obtained the first data on rovibrational energy levels of H_2O by dispersing visible sunlight attenuated by atmospheric water absorption and recording it photographically. Tens of thousands of transitions to levels with energies up to 25 500 cm^{-1} have been measured over the past few decades by using high-resolution Fourier transform (FT) spectrometers,[6−9] particularly by coupling them to long-path absorption cells of various types.[10] The FT approach has many advantages, particularly its high accuracy and spectral resolution and its broad spectral range. Yet, as in any type of direct absorption spectroscopy, its sensitivity is limited. The use of the cavity ring-down techniques[11−14] provides greatly improved sensitivity, enabling the detection of weak overtone transitions to water levels as high as 26 270 cm^{-1}, corresponding to the seventh stretch overtone.[15] Until recently, these were the highest measured levels of water, because the oscillator strength of overtone transitions drops by roughly an order of magnitude per each additional change in OH-stretch quantum. A large number of transitions, particularly those originating from high rotational levels, have been detected in the emission spectra of sunspots,[16] and laboratory experiments on hot water vapor[17] have verified and complemented these measurements, yielding positions of some previously unobserved levels below ∼25 000 cm^{-1}.

Both room-temperature absorption and hot emission spectra are usually fairly complicated, and their assignment relies heavily on theory and computations. Advanced theoretical models are capable of predicting many transitions in water with near spectroscopic accuracy over a wide range of rovibrational energy.[2,3,18,19] The most accurate calculations of rovibrational energy levels of water employ the variational method that sets up a rovibrational Hamiltonian by calculating the matrix elements of the exact kinetic energy operator with a potential energy surface (PES) in a suitable basis set. Numerical diagonalization of this matrix yields energy levels with an accuracy that is limited only by the quality of the employed PES. Deriving a PES for water that is capable of reproducing all measured levels and predicting unobserved levels with experimental accuracy remains the principle challenge for theoreticians. However, even the best potential surfaces are difficult to extrapolate accurately to geometries sampled at higher energy. Experimental determination of at least some energy levels in the region above 26 000 cm^{-1} is therefore crucial to ensure accurate prediction of unmeasured levels.

We recently reported measurements of rovibrational levels in the previously unreachable energy range 26 000−34 000 cm^{-1} by using double-resonance vibrational overtone excitation.[20] We added 62 of these levels to 544 previously known levels at lower energies and used them to morph the best available ab initio PES, resulting in a new semiempirical surface, PES_{12}, that reproduces all measured levels with accuracy better than 1 cm^{-1}. Before being able to use this empirical surface to calculate unmeasured energy levels, one must assess its accuracy in predicting various high-lying rovibrational levels of water over a wide energy range, particularly states with bending excitation.

The double-resonance scheme that we have employed thus far enables access to very high vibrational overtone levels from single rotational states.[21−24] Although the spectral simplification afforded by double-resonance greatly facilitates the assignment of spectra, it is not efficient in generating large data sets. Rotational selection rules limit access from each preselected rovibrational level in our double-resonance scheme to only a few overtone transitions over a range of several tens of inverse

* Corresponding author. E-mail: oleg.boiarkin@epfl.ch.
† École Polytechnique Fédérale de Lausanne.
‡ Institute of Applied Physics RAS.

10.1021/jp805849q CCC: $40.75 © 2008 American Chemical Society
Published on Web 09/30/2008

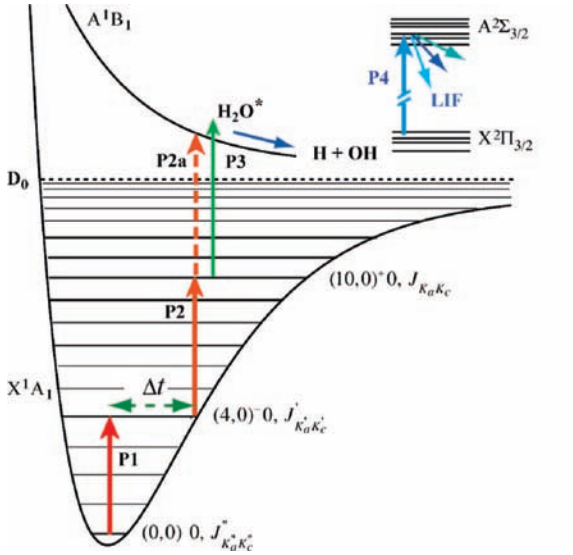

Figure 1. Energy level diagram for double-resonance excitation of the $(10,0)^+0$ vibration in H_2O (photons P1 and P2), with the subsequent transition to the A^1B_1 electronic repulsive state (P2a or P3) and the LIF detection of OH fragments (P4). A significant delay Δt between the two excitation pulses and an elevated pressure in CADROS experiments ensure collisional rotational relaxation.

centimeters, in contrast to classical absorption spectra, which typically contain several lines per inverse centimeter. One way to increase the number of transitions to highly excited states in our double-resonance scheme is to allow pre-excited molecules to undergo rotational relaxation from the intermediate rovibrational level before the arrival of the second excitation pulse. The variety of intermediate states thus created gives rise to many transitions to upper levels. We report here the use of this approach, which we call collisionally assisted double-resonance overtone spectroscopy (CADROS), to expand significantly our data set and test the accuracy of calculations by using our previously determined semiempirical PES.[20]

Experimental Approach

Figure 1 presents the energy-level scheme for rotationally selective double-resonance laser excitation to the $(10,0)^+0$ vibrational level of H_2O. Excitation of the 7th−11th OH-stretch overtones and stretch−bend combination levels (with a single bending quantum) from single rotational states employs similar schemes. The wavelength of the first pulsed laser (photon P1 in Figure 1) is tuned to a vibrational overtone transition from a single rotational level of the vibrational ground state and promotes a significant fraction of water molecules to an intermediate level that contains 4 (or 5) vibrational quanta in one of the OH-stretches. The known rotational assignment of the chosen transition[25,26] allows unambiguous determination of rotational quantum numbers of the intermediate level. After a delay of 8−10 ns, which, at typical pressures of 50 μbar, is short enough to ensure that no rotational relaxation occurs, a pulse from the second tunable laser irradiates the pre-excited molecules. Whenever the wavenumber of this laser (P2) is in resonance with a transition from the intermediate state, the pulse promotes up to half of the pre-excited molecules to a rovibrational state containing between 8 and 12 stretch quanta and up to 1 quantum of bend. Molecules in this terminal level are detected by vibrationally mediated photodissociation.[27,28] They first absorb either a UV/visible photon of the third pulsed laser (P3) or a second photon from the second excitation laser (P2a) that brings them to the repulsive A^1B_1 electronic surface. Subsequent prompt dissociation yields hot OH fragments with a broad rotational distribution because of the excess of energy over the dissociation threshold. In measurements of levels with $v_{str} \geq 10$, we delay the detection pulse (P4) by 100 ns with respect to the dissociation pulse (P2a) to allow for rotational relaxation of the hot OH fragments in collisions with room temperature H_2O. For $v_{str} < 10$, technical reasons limited us to leaving only 7 ns for OH relaxation before probing. The fourth laser pulse (P4) detects a fraction of OH fragments residing in the ground state ($X^2\Pi_{3/2}$, e, $J = 3/2$, $v = 0$) via laser-induced fluorescence (LIF) from the $A^2\Sigma_{3/2}$ electronic state. Monitoring OH fluorescence as a function of the wavenumber of the second laser (P2), while keeping the wavenumbers of all other lasers fixed, generates a photofragment spectrum of the overtone transition from the intermediate single rovibrational state to a terminal level.

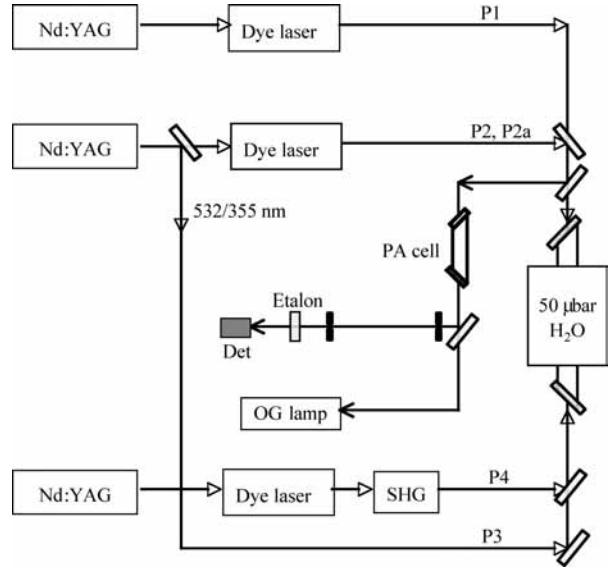

Figure 2. Optical layout of experiments.

In CADROS-type experiments, we intentionally increase the delay Δt between the first two laser pulses P1 and P2 (Figure 1) and/or the water-vapor pressure to allow significant rotational relaxation of H_2O in the intermediate level. The relaxation process prepares a variety of intermediate states but reduces the number of molecules per state in comparison with collision-free conditions, resulting in a lower signal-to-noise ratio. Two additional factors reduce this ratio: escape of the molecules in intermediate states from the laser-beam volume during the long delay and collisional quenching of electronically excited OH at elevated pressures. On the basis of our experimental observations, the optimal conditions occur when we increase the delay Δt (see Figure 1) up to 215 ns and the pressure up to 700 μbar. All other delays are set to 6−7 ns to minimize the loss of sensitivity.

Figure 2 shows the optical layout of the experimental setup. Three tunable laser pulses are generated by Nd:YAG (Spectra-Physics GCR-190, GCR-250) pumped dye lasers (Lumonics HD-500 and Lambda-Physic Scanmate) and have durations of 6−7 ns. The two overtone-pumping dye lasers (P1, P2) typically deliver 60−70 mJ at 20 Hz repetition rate. For LIF detection, the 3−5 mJ output of the third dye laser is frequency-doubled in a KDP crystal, which is mounted in an autotracker (Inrad, AT-II). The photolysis pulse (P3) results either from tripling (for the $v_{str} = 9$ and lower terminal levels) or doubling (for the terminal levels above v_{str}=9) a fraction of the fundamental

output of the same Nd:YAG that pumps the first of the dye lasers. Alternatively, for the υ_{str}=10 and higher terminal levels, photolysis can be performed by an additional photon of the second excitation laser.

The linearly polarized overtone excitation laser beams (P1, P2) pass through $F = +60$ cm lenses, which focus them to the center of a vacuum chamber. The two beams are then combined and sent to the chamber through a fused silica window, mounted at the Brewster angle. In the experiments on levels with $\upsilon_{str} < 11$, both beams have the same p-polarization and are combined on a dichroic mirror, except in the case of excitation to $\upsilon_{str} = 9$, where the beams of very close wavelength are combined on a partially reflecting dielectric mirror with 50% loss of their total energy. In experiments on levels with $\upsilon_{str} = 11-12$, the two excitation beams are orthogonally polarized and combined on a polarizing beam-splitter cube. The p-polarized photolysis laser beam (P3) and the UV detection beam (P4) are combined on a dichroic mirror and enter the chamber from the same side, counter-propagating with the overtone excitation beams (P1, P2). The UV beam used for LIF detection of OH is focused to the center of the chamber by an $F = 100$ cm lens and spatially filtered by a 0.5 mm pinhole placed 30 cm after the lens to reduce scattered light in the chamber. All beams are carefully overlapped inside the chamber. The emitted photons are collected by a condenser lens in the direction orthogonal to the beam axis and imaged onto a 10×1 mm^2 slit in front of a photo multiplier tube (PMT, EMI 6935QB). A band-pass glass filter (Hoya U-340) placed in front of the PMT suppresses visible laser scattered light and reduces that from UV detection laser (P4) but transmits most of the red-shifted near-UV fluorescence.

A small fraction of each dye laser beam is directed toward a Ne-filled hollow cathode optogalvanic lamp for absolute calibration of the lasers. For precise tuning of the first excitation laser to a desired overtone transition, it is sent through a water-vapor-filled photoacoustic cell. To correct for small discrepancies that may occur between the actual wavelength and the one reported by the laser control electronics during a laser scan, a small, well-collimated fraction of this laser beam is directed toward an air-spaced etalon with 1 cm^{-1} free spectral range. We record transmittance signal from a photodiode placed behind the etalon along with the LIF signal from the PMT.

Results

Figure 3 presents spectra of transitions to several high vibrational levels in H_2O obtained by double-resonance overtone excitation at water-vapor pressure of 50 μbar and a 10 ns delay between the two excitation pulses. Under these conditions, rotational relaxation during the overtone excitation process should be negligible. A common feature of these spectra is that they all originate from the same $J_{KaKc} = 1_{01}$ intermediate rotational state, although from two different vibrational levels ($\upsilon_{str} = 4$ and 5). Both excitation steps are governed by rotational selection rules, which strictly determine the change of angular momentum J ($\Delta J = 0, \pm 1$) and its projection onto z-axis of the laboratory frame M ($\Delta M = 0, \pm 1$). For high levels of vibrational excitation, K_a and K_c should be considered simply as notations rather than approximate quantum numbers because of the significant asymmetry of water molecule. Nevertheless, the strongest A-type and B-type transitions obey the $\Delta K_a = 0$, $\Delta K_c = \pm 1$ and the $\Delta K_a = \pm 1$, $\Delta K_c = \pm 1$ selection rules, respectively. The M selection rules, which are usually irrelevant to single-laser experiments, bring additional constraints in situations that employ sequential excitation by two linearly

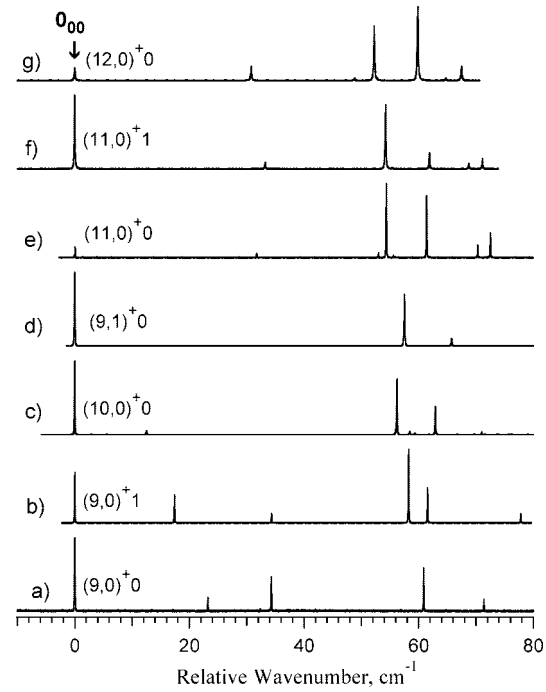

Figure 3. Double-resonance photofragment spectra of high rovibrational levels in H_2O plotted as a function of the total rovibrational energy and offset by the vibration band origins (a) 27 540.69 cm^{-1}, (b) 28 934.14 cm^{-1}, (c) 29 810.85 cm^{-1}, (d) 31 071.57 cm^{-1}, (e) 31 909.68 cm^{-1}, (f) 33 144.71 cm^{-1}, (g) 33 835.25 cm^{-1}. The intermediate state has been prepared by the following transition: (a−d) [(4,0)$^-$0, 1_{01}] ← [(0,0)0, 0_{00}] with orthogonal polarization of the two laser beams and (e−g) [(5,0)$^-$0, 1_{01}] ← [(0,0)0, 2_{02}] with parallel polarization of the two laser beams.

polarized laser beams. Parallel polarization of the two beams implies that the same component of the transition dipole moment is involved in two sequential transitions, whereas in the case of orthogonal polarizations, two laser fields interact with different components. Consideration of the transition matrix elements for different components of the dipole moment operator[29] indicates that the $J = 1 \leftarrow J' = 1 \leftarrow J'' = 0$ and $J = 0 \leftarrow J' = 1 \leftarrow J'' = 0$ two-step transitions are forbidden for the parallel and orthogonal polarizations, respectively. A comparison of two spectra originating from the same $J' = 1$ intermediate state but obtained with different relative polarizations of the excitation lasers makes the identification of vibrational band origins straightforward.

In the absence of collisional relaxation, the total energy of a terminal level is the sum of the rovibrational energy of intermediate state, which is known with high accuracy,[30] and the energy of the excitation photon (P2), which is measured to ± 0.03 cm^{-1} absolute accuracy. Collision-free double-resonance spectra of seven absorption bands yield energies of 185 states (Table 1, unlabelled values). We referred to these values in our earlier report of the semiempirical surface PES_{12}, which accurately reproduces all the levels between the ground state and 34 200 cm^{-1}. These values were used in fitting this surface, although we only reported 12 of them in ref 20.

A significant number of new transitions to high rovibrational levels appear in the CADROS-type spectra, shown in Figure 4. Under collision-free conditions, the transitions originate from the (4,0)$^-$0, 1_{01} rovibrational state, and terminate on the $\upsilon_{str} = 10$ level (Figure 4a). An increase of the collisional parameter, $p\Delta t$, increases relaxation of the initially prepared state up to the point of full rotational thermalization of the excited molecules. Moreover, at the maximum collisional parameter of

TABLE 1: Experimentally Determined Energy Levels of H_2O (in cm^{-1}) Labeled by Rotational J, K_a, K_c and Grouped by Vibrational $(m,n)^{\pm}b$ Quantum numbers

$(m,n)^{\pm}b = (6,1)^{-}3$	Δ(obs−calc) = ±0.28						
2 0 2	27560.50	3 1 2	27658.59	4 1 3	27745.49[b]	5 2 4	27906.96[b]
2 2 0	27619.30	4 0 4	27696.31[b]	5 1 5	27782.06		
$(m,n)^{\pm}b = (6,1)^{+}3$	Δ(obs−calc) = ±0.26						
0 0 0	27502.66	2 0 2	27563.88	2 2 0	27627.76	3 2 1	27734.20
1 0 1	27523.45	2 1 2	27579.70	3 0 3	27621.42	4 2 2	27824.19
1 1 1	27543.83	2 1 1	27598.75	3 1 2	27671.50	5 0 5	27780.07
1 1 0	27550.20	2 2 1	27626.23	3 2 2	27695.34	5 1 4	27880.15[b]
$(m,n)^{\pm}b = (9,0)^{-}0$	Δ(obs−calc) = ±0.22						
1 0 1	27557.13	3 2 2	27728.00	3 3 1	27784.65	4 3 1	27834.52
1 1 1	27575.80	2 2 1	27666.87	4 0 4	27730.77[b]	5 1 5	27821.08
2 0 2	27597.40	2 2 0	27668.90	4 1 4	27733.99	6 0 6	27923.91[b]
2 1 2	27611.71	3 1 3	27664.73	4 1 3	27767.50		
2 1 1	27627.53	3 1 2	27687.40	4 3 2	27833.48		
$(m,n)^{\pm}b = (9,0)^{+}0$	Δ(obs−calc) = ±0.37						
0 0 0	27540.69	3 0 3	27658.69	3 1 2	27700.10	5 0 5	27819.56
1 0 1	27561.27	2 1 2	27612.30	3 2 2	27727.17	5 1 5	27822.45[b]
1 1 1	27576.73	2 1 1	27630.82	4 1 4	27736.54[b]	6 3 4	28055.54[b]
1 1 0	27583.60	2 2 1	27666.76	4 2 3	27783.67		
2 0 2	27601.26	2 2 0	27668.23	4 2 2	27783.66		
$(m,n)^{\pm}b = (7,1)^{-}1$	Δ(obs−calc) = ± 0.27						
1 0 1	27582.67	1 1 0	27615.32	3 1 3	27696.17	5 1 5	27863.59
1 1 1	27609.80	2 0 2	27633.00	4 1 3	27807.01	6 0 6	27936.58[b]
$(m,n)^{\pm}b = (7,1)^{+}1$	Δ(obs−calc) = ±0.27						
0 0 0	27574.91	2 1 2	27647.10	3 2 2	27749.92	5 0 5	27859.78
1 0 1	27595.71	2 1 1	27667.54	3 2 1	27749.76	5 2 3	27974.42
1 1 1	27610.18	2 2 0	27723.93	4 1 3	27807.52[b]		
1 1 0	27616.80	3 0 3	27691.34	4 2 3	27870.28		
2 0 2	27636.38	3 1 2	27739.40	4 2 2	27869.25		
$(m,n)^{\pm}b = (9,0)^{+}1$	Δ(obs−calc) = ±0.24						
1 1 0	28938.66	2 1 2	28968.90	2 2 0	29011.93	5 0 5	29175.09
2 0 2	28951.53						
$(m,n)^{\pm}b = (9,0)^{-}1$	Δ(obs−calc) = ±0.52						
2 0 2	28950.91	2 1 2	28968.46	2 2 0	29012.20	5 1 5	29175.89
$(m,n)^{\pm}b = (7,1)^{+}2$	Δ(obs−calc) = ± 0.25						
0 0 0	28934.14	2 0 2	28992.39	2 1 2	28996.28	5 0 5	29220.97
1 1 0	28981.69						
$(m,n)^{\pm}b = (7,1)^{-}2$	Δ(obs−calc) = ±0.28						
2 0 2	28993.08	2 1 2	28995.68	2 2 0	29036.88		
$(m,n)^{\pm}b = (10,0)^{+}0$	Δ(obs−calc) = ±0.33						
0 0 0	29810.85	3 2 1	29975.75[b]	5 1 4	30128.24[b]	6 3 3	30328.90[b]
1 0 1	29829.87[b]	3 3 1	30028.91[b]	5 2 4	30139.73[b]	6 4 3	30396.78[b]
1 1 1	29839.49[b]	3 3 0	30029.09	5 2 3	30162.32	7 0 7	30284.78[b]
1 1 0	29843.39	4 0 4	29989.65[b]	5 3 3	30203.40[b]	7 1 7	30284.43[b]
2 0 2	29867.13	4 1 4	29991.46[b]	5 3 2	30207.06[b]	7 1 6	30371.96[b]
2 1 2	29873.74	4 1 3	30029.25[b]	5 4 2	30280.85[b]	7 2 5	30430.13[b]
2 1 1	29885.45[b]	4 2 3	30046.66	5 4 1	30280.73[b]	7 3 4	30473.06[b]
2 2 1	29914.11[b]	4 2 2	30058.62[b]	5 5 0	30378.61[b]	8 0 8	30412.86[b]
2 2 0	29915.13	4 3 2	30106.50[b]	6 0 6	30171.58	8 1 8	30412.92[b]
3 0 3	29920.79	4 3 1	30107.52[b]	6 1 6	30171.89[b]	8 1 7	30516.37[b]
3 1 3	29924.57[b]	4 4 0	30184.18[b]	6 1 5	30242.92[b]		
3 1 2	29947.78	5 0 5	30073.98	6 2 5	30249.46[b]		
3 2 2	29971.30[b]	5 1 5	30073.21[b]	6 3 4	30319.18[b]		
$(m,n)^{\pm}b = (10,0)^{-}0$	Δ(obs−calc) = ±0.34						
0 0 0	29810.87[b]	3 2 2	29971.32	5 0 5	30073.94[b]	6 2 4	30287.02[b]
1 0 1	29829.96[b]	3 2 1	29975.84[b]	5 1 5	30073.21	6 3 4	30318.95[b]
1 1 1	29839.51[b]	3 3 1	30028.94	5 1 4	30128.16[b]	6 3 3	30328.94[b]

TABLE 1: Continued

$(m,n)^{\pm}b$ = (10,0)$^{-}$3	Δ(obs−calc) = ±0.34						
1 1 0	29843.44[b]	3 3 0	30029.12[b]	5 2 4	30139.55[b]	6 4 2	30398.10[b]
2 0 2	29867.10	4 0 4	29989.61[b]	5 2 3	30162.55[b]	6 5 1	30494.60[b]
2 1 2	29873.76	4 1 4	29991.43[b]	5 3 3	30203.41[b]	7 1 7	30284.88[b]
2 1 1	29885.46[b]	4 1 3	30029.33	5 3 2	30207.16[b]	7 2 6	30375.62[b]
2 2 1	29914.17[b]	4 2 3	30046.78[b]	5 4 2	30280.19[b]	7 3 5	30453.47[b]
2 2 0	29915.12	4 2 2	30058.04[b]	6 0 6	30171.53[b]	8 1 7	30515.79[b]
3 0 3	29920.78[b]	4 3 2	30106.50[b]	6 1 6	30171.90[b]		
3 1 3	29924.55	4 3 1	30107.59[b]	6 1 5	30243.14[b]		
3 1 2	29947.84[b]	4 4 0	30184.62[b]	6 2 5	30249.35[b]		
$(m,n)^{\pm}b$ = (10,0)$^{+}$1	Δ(obs−calc) = ±0.39						
0 0 0	31071.57	2 0 2	31129.05	4 2 3	31316.30	5 0 5	31336.22
1 1 0	31106.68	2 1 2	31136.58	5 2 3	31438.12		
$(m,n)^{\pm}b$ = (10,0)$^{-}$1	Δ(obs−calc) = ± 0.39						
2 0 2	31129.93	2 2 0	31182.86	3 0 3	31183.88[b]	5 1 5	31335.22
2 1 2	31137.31						
$(m,n)^{\pm}b$ = (9,1)$^{+}$0	Δ(obs−calc) = ±0.65						
0 0 0	31207.09	2 0 2	31264.38	3 0 3	31318.51	5 0 5	31470.50
1 1 0	31241.17	2 1 2	31269.19[b]	4 2 3	31446.00		
$(m,n)^{\pm}b$ = (9,1)$^{-}$0	Δ(obs−calc) = ±0.07						
2 0 2	31264.26	2 1 2	31270.48	2 2 0	31312.73		
$(m,n)^{\pm}b$ = (11,0)$^{+}$0	Δ(obs−calc) = ±2.07						
0 0 0	31909.68	2 0 2	31964.00	3 0 3	32016.14	5 1 4	32215.37
1 0 1	31928.02	2 1 2	31971.01	3 1 2	32041.38[b]	5 3 2	32293.88
1 1 0	31941.33	2 2 0	32011.75	4 1 4	32085.40[b]		
$(m,n)^{\pm}b$ = (11,0)$^{-}$0	Δ(obs−calc) = ±2.07						
1 1 1	31937.38	2 1 2	31971.02	3 2 2	32065.90[b]	5 2 4	32228.30
1 1 0	31941.37	2 1 1	31981.63	4 0 4	32083.22[b]		
2 0 2	31963.97	2 2 1	32020.36				
$(m,n)^{\pm}b$ = (11,0)$^{+}$1	Δ(obs−calc) = ±0.18						
0 0 0	33144.71	2 0 2	33198.95	3 1 2	33279.42	5 2 3	33491.31[b]
1 0 1	33163.08	2 1 2	33206.58	4 1 4	33318.98[b]	5 3 2	33541.99
1 1 0	33177.92	3 0 3	33250.63	5 1 4	33454.52		
$(m,n)^{\pm}b$ = (11,0)$^{-}$1	Δ(obs−calc) = ±1.06						
1 1 1	33173.89	2 1 2	33206.58	3 1 3	33255.12	5 2 4	33468.19
1 1 0	33177.95	2 1 1	33218.83	3 2 1	33310.13[b]		
2 0 2	33198.96	2 2 0	33251.94	4 0 4	33316.74		
$(m,n)^{\pm}b$ = (12,0)$^{+}$0	Δ(obs−calc) = ±0.81						
0 0 0	33835.25	2 0 2	33887.44	3 0 3	33937.97	4 3 2	34116.71
1 0 1	33852.83	2 1 2	33895.08	3 1 2	33961.32	5 1 4	34128.24
1 1 0	33866.05	2 2 1	33933.44[b]	3 2 1	33990.19	5 3 2	34207.21
$(m,n)^{\pm}b$ = (12,0)$^{-}$0	Δ(obs−calc) = ±0.39						
0 0 0	33835.22	2 0 2	33887.46	2 2 0	33935.25	4 0 4	34003.30
1 1 1	33862.96	2 1 2	33895.08	3 1 3	33942.85	5 1 5	34084.87[b]
1 1 0	33866.04	2 1 1	33904.41[b]	3 2 2	33987.34	5 2 4	34143.36

[a] Standard deviation (in cm^{-1}) of the calculated values from those in the table is shown for each vibrational band. Nonmarked levels have been determined from the main (intense) peaks of the spectra, obtained at low pressure and with the shortest delays. [b] Additional levels determined from the CADROS spectra. Experimental accuracy of energy measurements is ± 0.03 cm^{-1}.

our experiment (Figure 4d), there should be appreciable vibrational relaxation.[31] This process can prepare a variety of ro-vibrational states at different energies, some of which are difficult to access by direct laser excitation (for instance, states with high bending excitation). However, the second and third photons (P2 and P2a) can access the repulsive electronic surface only from intermediate vibrational levels with $\upsilon_{str} \geq 3$, as one can estimate from the computed topology of the ground[32] and repulsive[33] surfaces. Therefore, only the transitions from these states can be detected and appear in the photodissociation spectra in Figure 4. Some of the transitions in the CADROS spectra of Figure 4 also appear as reproducible peaks of small intensity (0.2−2% of the largest peaks) in spectra similar to the one in Figure 3c, obtained at the smallest collisional parameter. Such

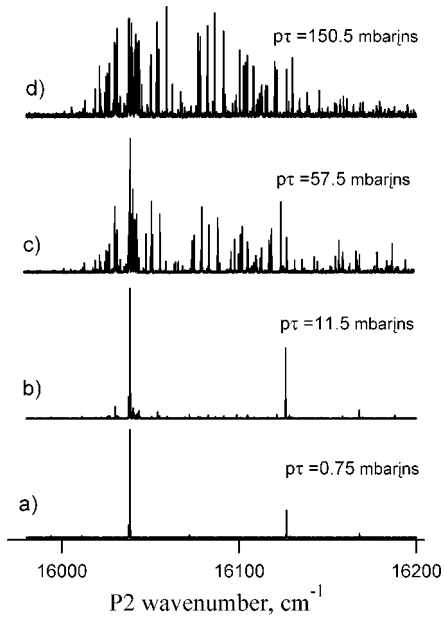

Figure 4. CADROS spectra of ortho-H_2O, obtained under increasing sample pressure P and time-delay τ between the two excitation pulses, (a) $p = 50$ μbar, τ=15 ns; (b) $p = 100$ μbar, τ=115 ns; (c) $p = 500$ μbar, τ=115 ns; (d) $p = 700$ μbar, τ=215 ns, and plotted as a function of the photon energy P2 of the second laser. Each spectrum is labeled by the collisional parameter, $p\tau$. The first laser is tuned to the transition $[(4,0)^-0, 4_{04}] \leftarrow [(0,0)0, 3_{03}]$ at 13 901.50 cm^{-1}.

peaks, which are observable only because of the high signal-to-noise ratio (>3000) in our experiment, suggest that a tiny fraction of molecules undergo rotational relaxation even under our collision-free conditions.

Two specific factors are to be considered for assignment of the CADROS spectra of Figure 4. First, all the involved states belong to the same ortho nuclear spin species, because they are accessed from the same initially prepared ortho state. To cover both nuclear species, we also obtained a CADROS spectrum by pumping the $(4,0)^+0$, 1_{11} intermediate para level under the conditions of the spectrum in Figure 4d. The spectra of the two nuclear spin species do not exhibit any of the same strong transitions. This indicates that no detectable collisional ortho−para spin relaxation occurs with $p\tau = 1.5 \times 10^{-10}$ bar•s. Moreover, pumping two different intermediate rotational levels of the ortho species ($(4,0)^+0$, 4_{04} and $(4,0)^+0$, 1_{11}) under the same conditions yields essentially the same spectrum, indicating the completeness of collisional rotational relaxation.

Second, because of collisional energy transfer, the total energy of a terminal level is the sum of the energy of the photon, P2, and that of the collisionallly prepared intermediate state rather than the initially prepared intermediate state. The identity of the collisionally prepared intermediate state comes from the assignment of the CADROS spectra, which became possible only after developing PES_{12}. We first use this surface to calculate a list of all possible transitions with $J \leq 8$ between energy levels lying up to 35 000 cm^{-1}. We then eliminate lines originating from states with $v_{str} < 3$, because our detection scheme will not see them (as described above) and assign all transitions between already known levels at $v_{str} = 3$, 4,[30] and 10.[20] This leaves few choices for the remaining transitions. Using combination differences and verifying that all allowed transitions from a given intermediate level appear with appropriate relative intensities allow us to complete the assignments. In total, 81 additional levels (labeled with the letter b in Table 1) have been obtained from assignment of just two (ortho and para) CADROS spectra.

For most of the vibrations, the average standard deviations of the calculated levels from the experimentally determined values is below 1 cm^{-1}, demonstrating the predictive capabilities of PES_{12}. A few relatively strong transitions, however, could not be assigned, and for $(11,0) \pm 0$ vibrational states, the standard deviation exceeds 2 cm^{-1}. One possible reason for this is that the PES_{12} originates from an ab initio PES that has been generated with points that do not cover the geometries of H_2O accessed at sufficiently high energy. The next step toward improving the accuracy of the theory is to perform high-level calculations of ab initio points at energies up to the dissociation threshold (including quasibound states above the threshold), and this work is in progress.

Conclusions

We employ a laser double-resonance overtone excitation scheme to measure energies of high rovibrational levels in H_2O, accessed from single rovibrational states. These levels are spread through the energy region 26 000−34 200 cm^{-1} and are difficult to access from the vibrational ground state by single-photon excitation because of the extreme weakness of such overtone transitions.

The CADROS approach significantly improves the productivity of double-resonance experiments and allows monitoring of transitions from states that are difficult to prepare by laser excitation. Two CADROS spectra alone allow the determination of 81 new rovibrational levels. The assignment of transitions in such spectra is challenging, however, and it is greatly assisted by calculations that employ our previously developed PES_{12}.

Comparison of experimentally determined energy levels with those calculated by using the PES_{12} surface suggests that these calculations are capable of predicting certain types of rovibrational levels (i.e, those with $J \leq 6$ and bending quantum numbers $v_b \leq 2$) with energy below ~34 000 cm^{-1} with accuracy better than 1 cm^{-1} on average. No collisional ortho−para spin relaxation in water vapor has been detected in the measured CADROS spectra, suggesting that such relaxation is slower than 6.7×10^9 bar^{-1} s^{-1}.

Acknowledgment. We thank the FNS (Grants no. 200020-112071 and 200021-117929/1), the EU (FP6 Grant no. 512202, QUASAAR), and the RFBR and RFP (Grant MK-1155.2008.2) for their generous support of this work.

Supporting Information Available: Ro-vibrational transitions from intermediate to terminal states, experimentally observed in double-resonance overtone excitation spectra of water molecule in the ground electronic state. This material is available free of charge via Internet at http://pubs.acs.org.

References and Notes

(1) *Climate Change 2007. The Physical Science Basis*; Solomon, S., Qin, D., Manning, M., Marquis, M., Averyt, K., Tignor, M. M. B., Miller, H. L., Chen, Z., Eds.; Cambridge University Press: Cambridge, 2007.

(2) Partridge, H.; Schwenke, D. W. *J. Chem. Phys.* **1997**, *106*, 4618.

(3) Polyansky, O. L.; Csaszar, A. G.; Shirin, S. V.; Zobov, N. F.; Barletta, P.; Tennyson, J.; Schwenke, D. W.; Knowles, P. J. *Science* **2003**, *299*, 539.

(4) Baumann, W.; Mecke, R. *Z.Physik* **1993**, *81*, 445.

(5) Mecke, R. *Z. Physik* **1933**, *81*, 313.

(6) Camypeyret, C.; Flaud, J. M.; Maillard, J. P.; Guelachvili, G. *Mol. Phys.* **1977**, *33*, 1641.

(7) Camypeyret, C.; Flaud, J. M.; Mandin, J. Y.; Chevillard, J. P.; Brault, J.; Ramsay, D. A.; Vervloet, M.; Chauville, J. *J. Mol. Spectrosc.* **1985**, *113*, 208.

(8) Mandin, J. Y.; Chevillard, J. P.; Camypeyret, C.; Flaud, J. M.; Brault, J. W. *J. Mol. Spectrosc.* **1986**, *116*, 167.

(9) Coheur, P. F.; Fally, S.; Carleer, M.; Clerbaux, C.; Colin, R.; Jenouvrier, A.; Merienne, M. F.; Hermans, C.; Vandaele, A. C. *J. Quant. Spectrosc. Radiat. Transfer* **2002**, *74*, 493.

(10) Carleer, M.; Jenouvrier, A.; Vandaele, A. C.; Bernath, P. F.; Merienne, M. F.; Colin, R.; Zobov, N. F.; Polyansky, O. L.; Tennyson, J.; Savin, V. A. *J. Chem. Phys.* **1999**, *111*, 2444.

(11) Macko, P.; Romanini, D.; Mikhailenko, S. N.; Naumenko, O. V.; Kassi, S.; Jenouvrier, A.; Tyuterev, V. G.; Campargue, A. *J. Mol. Spectrosc.* **2004**, *227*, 90.

(12) Kassi, S.; Macko, P.; Naumenko, O.; Campargue, A. *Phys. Chem. Chem. Phys.* **2005**, *7*, 2460.

(13) De Backer-Barilly, M. R.; Barbe, A.; Tyuterev, V. G.; Romanini, D.; Moeskops, B.; Campargue, A. *J. Mol. Struct.* **2006**, *780*, 225.

(14) Tanaka, M.; Sneep, M.; Ubachs, W.; Tennyson, J. *J. Mol. Spectrosc.* **2004**, *226*, 1.

(15) Dupre, P.; Gherman, T.; Zobov, N. F.; Tolchenov, R. N.; Tennyson, J. *J. Chem. Phys.* **2005**, *123*, 154307.

(16) Wallace, L.; Bernath, P.; Livingston, W.; Hinkle, K.; Busler, J.; Guo, B. J.; Zhang, K. Q. *Science* **1995**, *268*, 1155.

(17) Coheur, P. F.; Bernath, P. F.; Carleer, M.; Colin, R.; Polyansky, O. L.; Zobov, N. F.; Shirin, S. V.; Barber, R. J.; Tennyson, J. *J. Chem. Phys.* **2005**, *122*, 074307.

(18) Li, G.; Guo, H. *J. Mol. Spectrosc.* **2001**, *210*, 90.

(19) Shirin, S. V.; Polyansky, O. L.; Zobov, N. F.; Ovsyannikov, R. I.; Csaszar, A. G.; Tennyson, J. *J. Mol. Spectrosc.* **2006**, *236*, 216.

(20) Maksyutenko, P.; Muenter, J. S.; Zobov, N. F.; Shirin, S. V.; Polyansky, O. L.; Rizzo, T. R.; Boyarkin, O. V. *J. Chem. Phys.* **2007**, *126*, 241101.

(21) Boyarkin, O. V.; Rizzo, T. R. *J. Chem. Phys.* **1995**, *103*, 1985.

(22) Barnes, R. J.; Gross, A. F.; Sinha, A. *J. Chem. Phys.* **1997**, *106*, 1284.

(23) Boyarkin, O. V.; Rizzo, T. R.; Perry, D. S. *J. Chem. Phys.* **1999**, *110*, 11346.

(24) Maksyutenko, P.; Rizzo, T. R.; Boyarkin, O. V. *J. Chem. Phys.* **2006**, *125*, 181101.

(25) Tolchenov, R. N.; Naumenko, O.; Zobov, N. F.; Shirin, S. V.; Polyansky, O. L.; Tennyson, J.; Carleer, M.; Coheur, P. F.; Fally, S.; Jenouvrier, A.; Vandaele, A. C. *J. Mol. Spectrosc.* **2005**, *233*, 68.

(26) Rothman, L. S.; Jacquemart, D.; Barbe, A.; Benner, D. C.; Birk, M.; Brown, L. R.; Carleer, M. R.; Chackerian, C.; Chance, K.; Coudert, L. H.; Dana, V.; Devi, V. M.; Flaud, J. M.; Gamache, R. R.; Goldman, A.; Hartmann, J. M.; Jucks, K. W.; Maki, A. G.; Massie, S. T.; Orphal, J.; Perrin, A.; Rinsland, C. P.; Smith, M. A. H.; Tennyson, J.; Tolchenov, R. N.; Toth, R. A.; Vander-Auwera, J.; Varanasi, P.; Wagner, G. *J. Quant. Spectrosc. Radiat. Transfer* **2005**, *96*, 139.

(27) Hausler, D.; Andresen, P.; Schinke, R. *J. Chem. Phys.* **1987**, *87*, 3949.

(28) Vander Wal, R. L.; Crim, F. F. *J. Phys. Chem.* **1989**, *93*, 5331.

(29) Landau, L. D.; Lifshitz, E. M. *Quantum mechanics. Nonrelativistic theory*, 4th ed; Nayka: Moscow, 1989.

(30) Tennyson, J.; Zobov, N. F.; Williamson, R.; Polyansky, O. L.; Bernath, P. F. *J. Phys. Chem. Ref. Data* **2001**, *30*, 735.

(31) Barnes, P. W.; Sims, I. R.; Smith, K. M. *J. Chem. Phys.* **2004**, *120*, 5592.

(32) Barletta, P.; Shirin, S. V.; Zobov, N. F.; Polyansky, O. L.; Tennyson, J.; Csaszar, A. G. *J. Chem. Phys.* **2006**, *125*, 204307.

(33) Harrevelt, R. v.; Hermert, M. C. v. *J. Chem. Phys.* **2001**, *114*, 10.

JP805849Q